Magnetic Coils for a High-β Quasi-isodynamic Stellarator

W.A. Cooper[1], M. Drevlak[2], M.Yu. Isaev[3], M.I. Mikhailov[3], J. Nührenberg[2], V.D. Shafranov[3], A.A. Subbotin[3], R. Zille[2]

[1] *CRPP, Association Euratom-Confédération Suisse, EPFL, Lausanne, Switzerland*

[2] *Max-Planck-Institut für Plasmaphysik, IPP-EURATOM Association, Germany*

[3] *Russian Research Centre "Kurchatov Institute", Moscow, Russia*

Abstract Previously it was shown by computational optimization that a quasi-isodynamic (qi) [1,2] configuration exists with $N = 6$, $A = 12$ [3] in which good α-particle collisionless confinement, small neoclassical transport and small bootstrap current can be achieved simultaneously with a high stable β value, $\langle\beta\rangle \approx 9\%$. In the approach used, the configuration was defined by a boundary magnetic surface. To find out whether this configuration can be realized by magnetic coils with acceptable complexity, the NESCOIL/ONSET suite of codes [4 - 7] was used to carry out a coil design. In this paper preliminary results are reported. The properties of the resulting free-boundary equilibrium are calculated and compared with those of the initial configuration.

Introduction Quasi-isodynamic configurations were introduced in Ref. [1] as those in which deeply to moderately deeply reflected particles are confined by poloidal closure of their banana orbit drifts, i.e. the second adiabatic invariant $\mathcal{J}_{||} = \int v_{||} dl$ is approximately constant on a magnetic surface. It was shown later by computational optimization that the qi condition can be satisfied with high accuracy for all reflected particles [2]. By definition, approximating qi should lead to improvement of fast-particle confinement and diminished neoclassical transport. In addition, it can be shown analytically [3] that in exact qi configurations the bootstrap current should be negligible.

Hence, qi allows for the simultaneous improvement of several stellarator properties. This was confirmed by computational optimization. By integrated optimization, the boundary magnetic surface providing the optimization space, a six-period configuration was found that simultaneously exhibits very good long-time collisionless α-particle confinement, small neoclassical transport, negligible bootstrap current and high stable β value [3].

The experimental viability of this configuration hinges upon the feasibility of a suitable coil configuration. Here, preliminary results of a coil design are reported. The properties of the associated free-boundary equilibrium found are compared with those of the initial optimized equilibrium.

Coil design The coil optimisation was carried out using the NESCOIL/ONSET suite of codes described in [4, 5]. Due to the high $\langle\beta\rangle$ the coil design has to include the effect of the plasma currents. For this purpose, a procedure similar to [6] was employed, which includes the plasma field on the plasma boundary when minimising the field error. However, in contrast to the original method, the field from the plasma currents was given not only on the design plasma boundary, but in a 3d region encompassing the entire plasma domain. This plasma field was generated using the EXTENDER_P code described in [7]. Using the magnetic field from plasma currents in the entire confinement domain, ONSET is able to optimise not only for the field error on the plasma boundary, but also for integral field line properties like location of the magnetic axis and axis ι. Note that this optimisation of field line properties is not founded on

an equilibrium solution consistent with the actual coil set. Still, it is capable of yielding improved results over an "unguided" optimisation at little additional computational cost.

The coil design uses 5 modular coils per half period situated off the symmetry planes. The optimisation used surfaces located 0.3 m and 1.2 m off the plasma boundary as constraining surfaces for the current carrying surface (CCS). Fig. 1 shows the constraining surfaces together with the optimised CCS and the plasma boundary. One period of the final coil design is shown in Fig. 2.

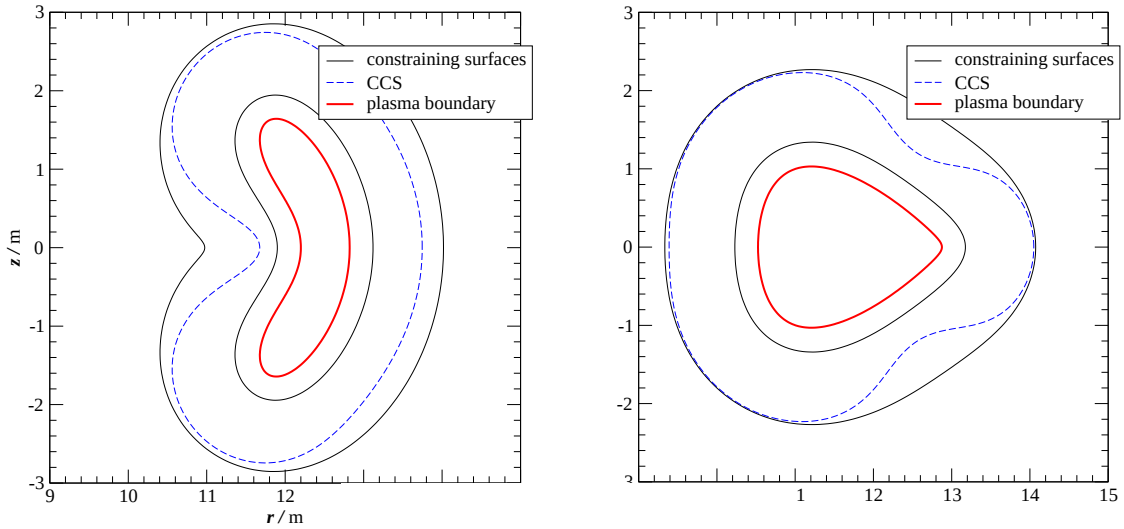

Fig. 1. Inner and outer constraining surface for the CCS, together with final CCS and plasma boundary. Shown are bean-shaped and the triangle-shaped cross section.

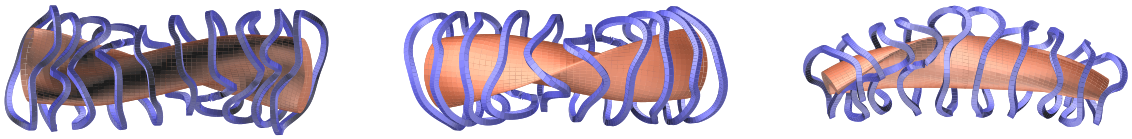

Fig. 2. Inner, outer and birds eye view of one period of the final coil system.

Comparison of properties of free-boundary and initial equilibria In the discussion below we refer to the initial equilibrium described in Ref. [3] as "fixed-boundary" case, and to the one realized by coils as the "free-boundary" case. Fig. 3 shows the differences in cross-sections for fixed- and free-boundary cases. Fig. 4 compares the design iota profile with the result from the free-boundary VMEC calculations obtained with the coils designed. It is seen that the free-boundary high-β equilibrium reproduces the original configuration with good accuracy as far as plasma cross-sections and rotational transform profile are concerned.

Fig. 5 shows the Mercier- and resistive-mode stability properties for both cases. For the fixed-boundary equilibrium Mercier- and resistive-interchange modes are marginally stable in the outer region of the plasma column. For the free-boundary equilibrium only the resistive-interchange modes become slightly unstable in the outer part of the plasma domain.

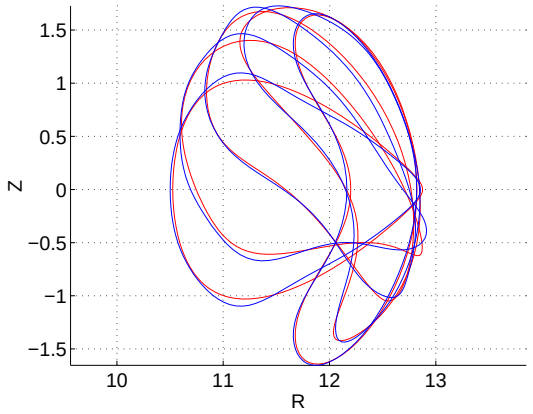

Fig. 3. Cross-sections of fixed- (red) and free-boundary (blue) equilibrium.

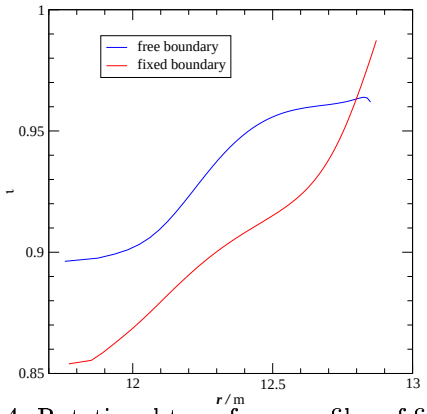

Fig. 4. Rotational transform profiles of fixed- (red) and free-boundary (blue) equilibrium.

The properties related to the particle drift motion were analysed, too. Fig. 6 shows the history of collisionless losses of 1000 α-particles launched at 1/2 of the minor plasma radius for power plant parameters (volume $V = 1000m3$, $B = 5T$). Losses only occur after long time of flight showing that there are no prompt losses. Correspondingly, the contours of the second adiabatic invariant are well closed inside the plasma column, as is seen in Fig. 7. Here, these contours are shown for a set of $B_{reflect} = B_{min} + i\Delta B/7$, $i = 1, ..., 6$, where ΔB is the variation of B at the normalised flux of $s_0 = 1/4$. Red colour corresponds to the highest $\mathcal{J}$ showing a maximum of $\mathcal{J}$ – created by the diamagnetic equilibrium current – near the magnetic axis. As β decreases this maximum becomes more and more shallow. Hence, a gradual increase of collisionless particle losses is expected as β decreases. For free-boundary equilibria with $\langle\beta\rangle = 4.4\%$ and $\langle\beta\rangle = 2.2\%$ the losses of α-particle are almost the same ($\approx 6\%$ of all particles) and approximately doubled, respectively. For particles started at $s_0 = 1/16$ (i.e. at a quarter of the radius) the losses for $< \beta >= 2.2\%$ are still small (2% after 1 second). The lines in Fig. 6 show the fractions of reflected particles ($\approx 45\%$).

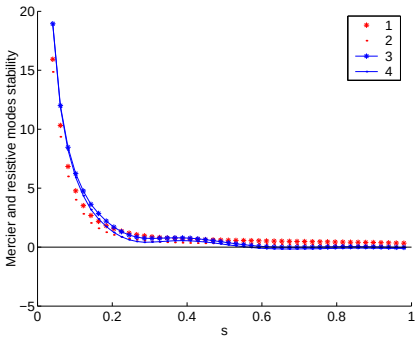

Fig. 5. Radial profiles of Mercier (1,3) and resistive-interchange criteria (2,4) for fixed- (1,2) and free-boundary (3,4) equilibrium.

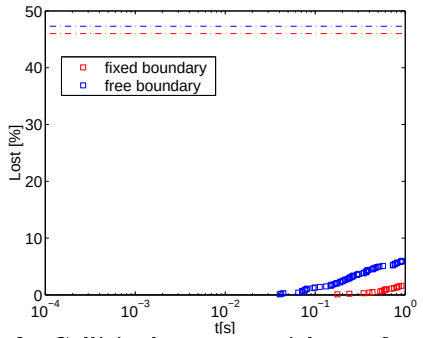

Fig. 6. Collisionless α-particle confinement as a function of time. The particles were launched at $s_0 = 1/4$.

The contours of the magnetic field strength on magnetic surfaces are largely poloidally closed (see Fig. 8), except for small residual islands near $B = B_{max}$. These small islands give rise to a small fraction of transitional (nonadiabatic) orbits that can be lost eventually.

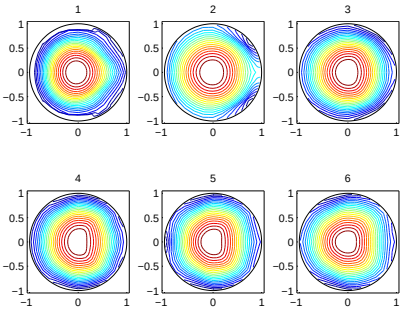

Fig. 7. Contours of the second adiabatic invariant $\mathcal{J}$ in polar representation $(\sqrt{s}, \theta_B)$ for a set of $B_{reflect}$.

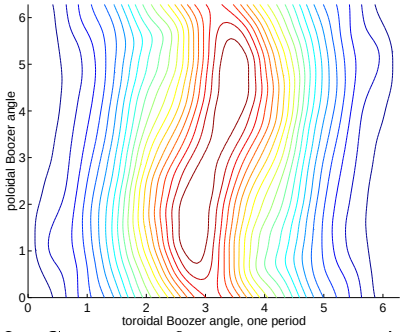

Fig. 8. Contours of constant magnetic field strength in magnetic coordinates.

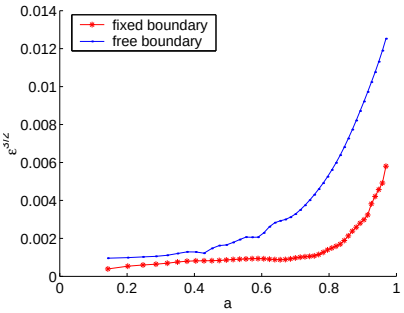

Fig. 9. Radial profiles of effective ripple for fixed- and free-boundary equilibria.

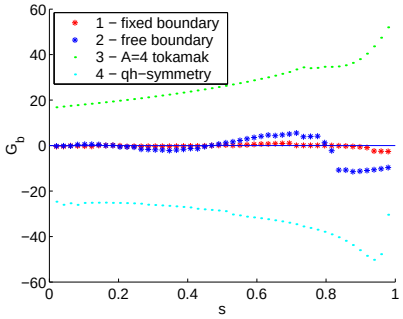

Fig. 10. Radial profiles of bootstrap current structural factor G_b for fixed- (1) and free-boundary (2) equilibria.

Fig. 9 shows the radial profiles of effective ripple obtained as described in [8]. In Fig. 10, the structural factor of the bootstrap current in the low-collisionality regime is plotted for the fixed- and free-boundary cases. For comparison, the structural factors for a tokamak with aspect ratio $A = 4$ (curve (3)) and for a quasihelically-symmetric configuration described in [9] (curve (4)) are shown, too.

Conclusions Preliminary results of the coil design presented show that the investigated properties of the design configuration can be approximated by modular coils of reasonable complexity. Further work is required to incorporate into the coil design the influence of resonances in the magnetic field on its structure.

References

[1] Gori S., Lotz W., Nührenberg J., Theory of Fusion plasmas (International School of Plasma Physics), Bologna: SIF (1996) 335.

[2] M.I. Mikhailov et al, *Nuclear Fusion* **42** 2002 L23.

[3] A.A. Subbotin et al, "Integrated Physics Optimization of a Quasi-isodynamic Stellarator with Poloidally Closed Contours of the Magnetic Field Strength", submitted to *Nucl. Fusion*.

[4] Merkel, P., Nucl.Fusion **27** (1987) 867.

[5] Drevlak, M., Fusion Technol. **33** (1998) 106.

[6] Merkel P., Drevlak, M., 1998 ICPP&25th EPS Conf. on Contr. Fusion and Plasma Physics, Praha, 29 June - 3 July, ECA Vol. 22C (1998) 1745-1748.

[7] Drevlak, M., Monticello, D., Reimann, A., Nucl. Fusion **45** (2005) 731-740.

[8] Nemov V.V. et al, *Plasma Phys. Control. Fusion* **45** (2003) 43.

[9] Nührenberg J. and Zille R., *Phys. Lett. A* **129** (1988) 113.